

THE *HERSCHEL* FILAMENT: A SIGNATURE OF THE ENVIRONMENTAL DRIVERS OF GALAXY EVOLUTION DURING THE ASSEMBLY OF MASSIVE CLUSTERS AT $Z=0.9^*$

K. E. K. COPPIN¹, J. E. GEACH^{1,2}, T. M. A. WEBB¹, A. FALOON¹, R. YAN³, D. O'DONNELL¹, N. OUELLETTE⁴, E. EGAMI⁵, E. ELLINGSON⁶, D. GILBANK⁷, A. HICKS⁸, L.F. BARRIENTOS⁹, H.K.C. YEE¹⁰, AND M. GLADDERS¹¹

Draft version March 2, 2012

ABSTRACT

We have discovered a 2.5 Mpc (projected) long filament of infrared-bright galaxies connecting two of the three $\sim 5 \times 10^{14} M_{\odot}$ clusters making up the RCS 2319+00 supercluster at $z = 0.9$. The filament is revealed in a deep *Herschel* Spectral and Photometric Imaging REceiver (SPIRE) map that shows 250–500 μm emission associated with a spectroscopically identified filament of galaxies spanning two X-ray bright cluster cores. We estimate that the total (8–1000 μm) infrared luminosity of the filament is $L_{\text{IR}} \simeq 5 \times 10^{12} L_{\odot}$, which, if due to star formation alone, corresponds to a total SFR $\simeq 900 M_{\odot} \text{ yr}^{-1}$. We are witnessing the scene of the build-up of a $> 10^{15} M_{\odot}$ cluster of galaxies, seen prior to the merging of three massive components, each of which already contains a population of red, passive galaxies that formed at $z > 2$. The infrared filament demonstrates that significant stellar mass assembly is taking place in the moderate density, dynamically active circumcluster environments of the most massive clusters at high-redshift, and this activity is concomitant with the hierarchical build-up of large scale structure.

Subject headings: Galaxies: clusters: individual (RCS 231953+0038.0, RCS 232002+0033.4, RCS 231948+0030.1) — Galaxies: high-redshift — Galaxies: starburst — Infrared: galaxies — Submillimeter: galaxies

1. INTRODUCTION

The average rate of galaxy growth, measured by the volume averaged star formation rate (SFR), was a factor of ~ 10 higher at $z \sim 1$ than it is today (e.g., Hopkins & Beacom 2006), when the environments destined to become the most massive ($10^{15} M_{\odot}$) clusters were still in the process of assembly. What effect does the growth of large scale structure at $z \sim 1$ have on the star formation histories of galaxies bound to, or being accreted onto, such environments? For over 30 years it has been known that the fraction of blue star-forming galaxies in clusters was higher in the past (Butcher & Oemler 1978, 1984), and more recent work has extended star formation surveys of distant clusters into the infrared (IR) regime (important for tracking the total SFR), reinforcing the view that there

has been strong evolution in the total SFR of clusters since $z \sim 1$ (e.g., Geach et al. 2006; Bai et al. 2009). To some extent the evolution seen in cluster populations tracks the field, but it is important to consider the environmental context of this evolution (e.g., Gilbank & Balogh 2008), since star-forming galaxies within high- z clusters are destined to evolve into the ‘red sequence’ in the cores of the descendants of such environments today (e.g., Gilbank et al. 2008a; Poggianti et al. 2008).

It is becoming clear that clusters exist at $z \sim 1$ that already contain an established population of massive galaxies that formed their stellar populations quickly at much higher redshifts ($z > 2$) when the cluster was in a much earlier state of collapse (e.g., Papovich et al. 2010). While this rapid formation episode puts in place the massive tail of the cluster galaxy population, the dwarf end of the red sequence undergoes significant evolution via the continuous accretion of satellite galaxies, with the bulk of such assimilation in the form of dwarf galaxies at $z = 0$, steepening the faint-end slope of the luminosity function (e.g., De Lucia et al. 2004; Gilbank et al. 2008a). What is the intermediate stage of red-sequence evolution at $z \sim 1$ and what role, if any, does the *assembly* of the clusters themselves play on their member galaxies? For example, is star formation triggered by, or at least associated with, the peripheral environments (outlying groups and filaments) feeding those massive clusters?

In this Letter we discuss observations performed with the ESA *Herschel Space Observatory* (Pilbratt et al. 2010) Spectral and Photometric Imaging REceiver (SPIRE; Griffin et al. 2010). We have discovered a remarkable filament of far-IR bright galaxies linking two of three massive clusters in close proximity at $z = 0.9$ – the RCS 2319+00 supercluster (Gilbank et al. 2008b). Our study reveals a glimpse of the process of galaxy evolution that is coeval with the birth of one of the most massive structures in the Universe; a text-book example of structure assembly in the hierarchical paradigm. We assume cosmological parameters of $\Omega_{\Lambda} = 0.73$, $\Omega_{\text{m}} = 0.27$,

**HERSCHEL* IS AN ESA SPACE OBSERVATORY WITH SCIENCE INSTRUMENTS PROVIDED BY EUROPEAN-LED PRINCIPAL INVESTIGATOR CONSORTIA AND WITH IMPORTANT PARTICIPATION FROM NASA.

¹ Department of Physics, McGill University, 3600 Rue University, Montréal, QC, H3A 2T8, Canada

² Banting Fellow

³ Center for Cosmology and Particle Physics, Department of Physics, New York University, 4 Washington Place, New York, NY, 10003, USA

⁴ Department of Physics, Engineering Physics & Astronomy, Queen's University, Kingston, ON, K7L 3N6, Canada

⁵ Steward Observatory, University of Arizona, 933 N. Cherry Ave, Tucson, AZ 85721, USA

⁶ Center for Astrophysics and Space Astronomy, Department of Astrophysical and Planetary Sciences, UCB-389, University of Colorado, Boulder, CO, 80309, USA

⁷ South African Astronomical Observatory, P.O. Box 9, Observatory, 7935, South Africa

⁸ Department of Physics and Astronomy, 3255 Biomedical and Physical Sciences Bldg., Michigan State University, East Lansing, MI, 48824-2320, USA

⁹ Departamento de Astronomía y Astrofísica Pontificia Universidad Católica de Chile, Vicuña Mackenna 4860, 7820436 Macul, Santiago, Chile

¹⁰ Department of Astronomy & Astrophysics, University of Toronto, 50 St. George St., Toronto, ON, M5S 3H4, Canada

¹¹ Department of Astronomy & Astrophysics, University of Chicago, 5640 S. Ellis Ave, Chicago, IL, 60637, USA

and $H_0 = 71 \text{ km s}^{-1} \text{ Mpc}^{-1}$ (Spergel et al. 2003).

2. RCS 2319+00

RCS 231953+0038.0 (hereafter RCS 2319+00) was detected in the first Red-Sequence Cluster Survey (RCS-1; Gladders & Yee 2005). Subsequent follow-up observations with *Chandra* (Hicks et al. 2008) and an extensive optical and near-IR spectroscopic campaign (Gilbank et al. 2008b; A. Faloon et al., 2012 in preparation; R. Yan et al., 2012 in preparation) have revealed a remarkable supercluster system (RCS 231953+0038.0, RCS 232002+0033.4, RCS 231948+0030.1) comprising three distinct X-ray luminous cores with $L_X \sim 3.6\text{--}7.6 \times 10^{44} \text{ erg s}^{-1}$, separated by $< 3 \text{ Mpc}$ in the plane of the sky and $\sim 10 \text{ Mpc}$ along the line of sight (assuming a Hubble flow). X-ray, strong lensing and virial mass estimates all imply individual cluster masses of $\sim 5 \times 10^{14} M_\odot$. The close proximity of the three components, taken with the fact that the extended X-ray emission and density profiles of the red-sequence members appear to be aligned strongly suggests that the clusters are most likely in the early stages of a three-way merger that will result in a $> 10^{15} M_\odot$ cluster by $z = 0.5$ (Gilbank et al. 2008b).

3. OBSERVATIONS AND DATA REDUCTION

3.1. *Herschel* data

RCS 2319+00 was observed with *Herschel* SPIRE using the ‘Large Map’ mode on 2009 December 17 as part of the *Herschel* Lensing Survey (OD 217; OBSID 1342188181; Egami et al. 2010). The scan direction was set to scan angles A and B, with the length and height of the map set to $4'$, yielding a map $17' \times 17'$ in extent, with a total observing time of 1.7 hr and on-source integration time of 0.6 hr (17 s per pixel). The data were reduced with the latest version of the *Herschel* interactive processing environment (HIPE v7.3.0; Ott 2010), including the use of the sigma-kappa deglitcher which showed improvement over the default routine. The maps have default pixel scales of 6, 10, and $14''$ at 250, 350, and $500 \mu\text{m}$, respectively. The HIPE *SUSSEX*tractor task (Savage & Oliver 2007) was used to produce match-filtered maps (raw maps convolved with a point spread function (PSF) of 18, 25, and $36''$ at 250, 350, and $500 \mu\text{m}$, respectively) and signal-to-noise ratio (SNR) > 3 source catalogs. The 1σ rms instrumental noise in the match-filtered maps is $\simeq 1.1$, 1.1, and 1.7 mJy at 250, 350, and $500 \mu\text{m}$, respectively. When quoting flux uncertainties, we add in quadrature to the instrumental noise a nominal confusion noise of $\simeq 5.8$, 6.3, and 6.8 mJy at 250, 350, and $500 \mu\text{m}$, respectively (Nguyen et al. 2010). The weighted SPIRE map means are consistent with 0 mJy.

3.2. *Spitzer* data

RCS-1 imaging and photometry catalogs from the $24 \mu\text{m}$ Multiband Imaging Photometer for *Spitzer* (MIPS; Rieke et al. 2004) are presented in T. Webb et al. (2012, in preparation). The MIPS coverage is complete down to $\simeq 96 \mu\text{Jy}$; for comparison, a local IR luminous galaxy, or LIRG, would be $\gtrsim 114 \mu\text{Jy}$ at the cluster redshift. *Spitzer* InfraRed Array Camera (IRAC; Fazio et al. 2004) four-channel imaging was obtained through programs 30940 and 50720 and reaches $M_K^* + 1.5$ at $z = 0.9$ and covers approximately the same area as the $24 \mu\text{m}$ observations. Image processing was performed using IRACPROC (Schuster, Marengo & Patten 2006), software developed to wrap the existing MOsaicking and Point-source EXtraction (MOPEX) pipeline in IRAC

mode and add IRAC-specific improvements to outlier rejection. Source detection and aperture photometry were performed using the Picture Processing Package (PPP; Yee 1991).

4. AN INFRARED-BRIGHT FILAMENT

All three SPIRE maps show a region of apparent ‘enhanced’ far-IR emission over the background – in the form of a complex of blended and confused point sources – spanning the ‘A’ and ‘B’ components of RCS 2319+00, but not extending into the core region of component ‘A’. For our analysis, we have defined a region encompassing the filament, described by the zone within $90''$ of a locus spanning the A–B cluster components (see Fig. 1). We discuss the significance of this emission below, but note that we cannot rule out the possibility that it is the result of an overlap of the outer regions of clusters A and B, rather than a true filament. However, we note that no similar structure is seen between cluster cores B and C which are similarly aligned on the sky, and the filament does not appear to run directly between the A and B cores, but rather traces an easterly arc (in both spectroscopy and SPIRE emission), suggestive of a real and unique structure. In addition, the existence of the structure is supported by coincident overdensities of spectroscopic cluster members and MIPS $24 \mu\text{m}$ number counts.

Based on extensive spectroscopy (> 2000 spectra) over the RCS 2319+00 structure with the VLT VIMOS and Magellan IMACS instruments (A. Faloon et al., 2012 in preparation; R. Yan et al., 2012 in preparation), A. Faloon et al. (2012, in preparation) have identified 14 $24 \mu\text{m}$ spectroscopically confirmed cluster members in the filament with $0.8700 < z < 0.9247$ and $(43 \pm 18) < S_{24} < (511 \pm 21) \mu\text{Jy}$. This redshift range was chosen to encompass the entire supercluster structure, based on the spectroscopic overdensity in Faloon et al. (2012, in preparation). We find that the filament has a $\simeq 2\times$ higher confirmed spectroscopic member density compared with regions in the surrounding $10 \times 10 \text{ arcmin}^2$ ‘field’ area, with a significance of 2.5σ . While our errors above do not take into account spectroscopic completeness, we have attempted to minimize any bias in our comparison by limiting the analysis to ‘field’ regions with similar spectroscopic sampling (ie., ~ 4 slits arcmin^{-2}) as the filament region and by also removing cluster members within 1 arcmin (0.5 Mpc) of the cluster cores. A more detailed analysis will be presented by A. Faloon et al. (2012, in preparation). There is also an apparent $\simeq 3\sigma$ hint of an overdensity of $24 \mu\text{m}$ sources in the filament ($N_{24} = (11.4 \pm 0.6) \text{ arcmin}^{-2}$) versus the immediate background ($N_{24} = (9.6 \pm 0.2) \text{ arcmin}^{-2}$).

To get a sense of the significance of the apparent far-IR enhancement within the filament as revealed by *Herschel*, we can simply sum the flux densities of the $\text{SNR} > 3\sigma$ $250 \mu\text{m}$ sources. However, note that point source extraction is inherently insensitive to blended and confused SPIRE sources and to extended emission, and thus our estimate will only yield a lower limit to the true level of far-IR emission if all of the emission seen is originating in the filament structure. To account for the apparent diffuse emission in the filament region, we plot a pixel flux histogram of the filament versus the background, showing a striking excess of far-IR emission in the filament at all flux levels (see Fig. 2). We now sum the 29 $250 \mu\text{m}$ sources in the filament region and subtract a conservative area-normalized background estimate (based on the flux density of $\text{SNR} > 3$ sources outside of the filament region), yielding $S_{250} = 281 \pm 33 \text{ mJy}$. Due to the incompleteness in

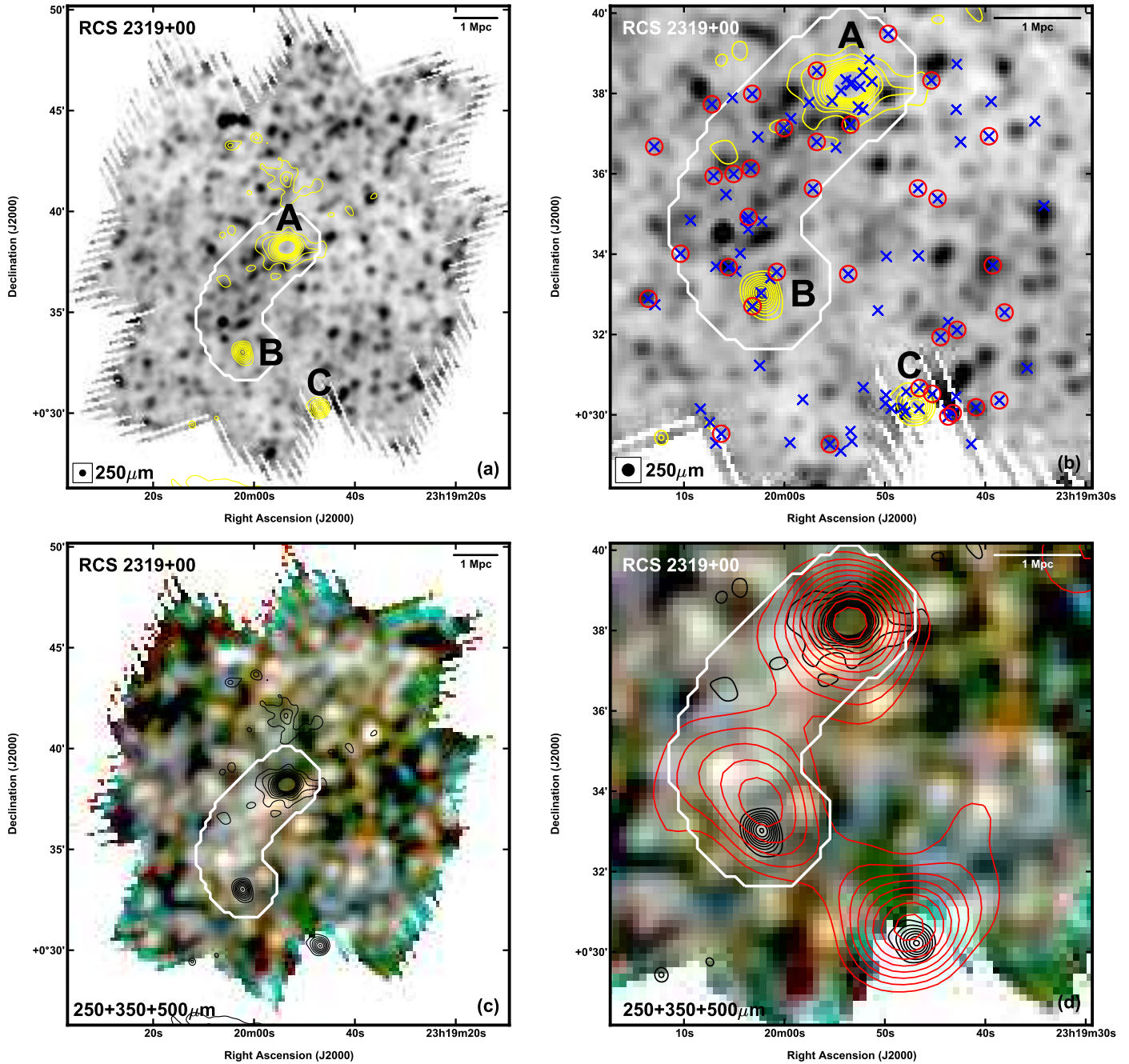


FIG. 1.— The *Herschel* filament in RCS 2319+00. The white outline indicates the filamentary region defined for the analysis, spanning components A–B, and is overlaid on the $250\ \mu\text{m}$ SPIRE map (*panels a and b*) and on an RGB composite of the 250 , 350 and $500\ \mu\text{m}$ maps smoothed to the lowest resolution (*panels c and d*). Smoothed X-ray emission contours (with the point-sources removed) are overplotted in yellow (*panels a and b*) or in black (*panels c and d*). *Panel b*) Blue ‘x’ symbols indicate the positions of the 41 confirmed $0.8700 < z < 0.9247$ cluster members, and are circled in red if they are $24\ \mu\text{m}$ -detected. *Panel d*) The red contours trace the surface density of galaxies selected by the RCS selection of ‘red-sequence’ galaxies at $z \sim 0.9$. As pointed out in Gilbank et al. (2008b), note that the major axis of the red-sequence clusters tends to point towards its nearest neighbour, and also notice the striking offset from the red-sequence defined cluster cores ‘B’ and ‘C’ to the peaks of the X-ray emission.

our source extraction, unsurprisingly we see only a $\simeq 2\sigma$ hint of an overdensity in the filament ($N_{250} = (1.1 \pm 0.2)\ \text{arcmin}^{-2}$) versus the background ($N_{250} = (0.7 \pm 0.05)\ \text{arcmin}^{-2}$).

We now present a more quantitative analysis and interpretation of the level of star-formation enhancement in the far-IR filament using our collection of extensive follow-up spectroscopy in RCS 2319+00.

4.1. Total infrared emission and star formation rate in the filament

We can estimate the contribution of far-IR emission in the filament by summing the far-IR flux densities of individual IR-bright cluster members and then scaling an appropriate galaxy spectral energy distribution (SED). To identify IR-bright cluster members we work directly with the MIPS $24\ \mu\text{m}$ imaging which has a much smaller PSF ($\text{FWHM} \simeq 6''$) than the SPIRE data and therefore allows for reliable cross-referencing with the spectroscopy. We then determine the appropriate far-IR SED shape by performing a standard stacking analysis (e.g. Marsden et al. 2009; Pascale et al. 2009) to de-

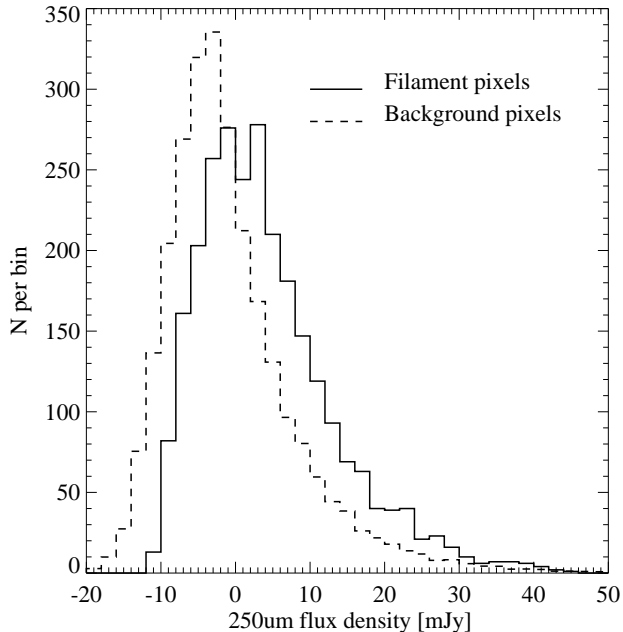


FIG. 2.— Area-normalized 250 μm pixel flux histograms showing a striking excess of far-IR emission in the filament versus the background (pixels outside the filament region).

rive the average three-band SPIRE flux densities of the 24 μm -detected cluster members in the filament, thus yielding the average SED from 24–500 μm .

The SPIRE imaging is much shallower relative to the MIPS imaging, and is only sensitive to $L_{\text{IR}} \gtrsim 10^{12} L_{\odot}$ activity at the cluster redshift – and indeed only three of the 24 μm cluster members appear to be ‘detected’ at 250 μm (see Fig. 1). We thus proceed to stack the flux densities from the SPIRE maps at the location of the 14 MIPS cluster members (which have an average 24 μm flux of $\simeq 170 \mu\text{Jy}$), yielding significant stacked flux densities of $11.0 \pm 1.6 \text{ mJy}$ (7.0σ), $10.7 \pm 1.7 \text{ mJy}$ (6.2σ), and $8.5 \pm 1.9 \text{ mJy}$ (4.6σ) at 250, 350, and 500 μm , respectively. We note that stacking the cluster members on the SPIRE maps using the much more precise MIPS positions should help to minimize any blending and confusion contamination from the SPIRE emission of non-cluster members. Fig. 3 shows the stacked SPIRE flux densities in relation to a set of spectral templates (Dale & Helou 2002) and the median *Herschel*-Astrophysical Terahertz Large Area Survey (H-ATLAS; Eales et al. 2010) galaxy template with $1 \times 10^{11} L_{\odot} < L_{\text{dust}} < 3 \times 10^{11} L_{\odot}$ from Smith et al. (2012), redshifted to $z = 0.9$ and normalized to the 250 μm stacked flux density. The far-IR colors are consistent with the ‘cool’ templates from the Dale & Helou (2002) library, with $S_{60}/S_{100} \lesssim 0.26$ rest-frame colors. The H-ATLAS template is also a reasonable fit to the average far-IR emission, yielding $L_{\text{IR}} = (1.9 \pm 0.3) \times 10^{11} L_{\odot}$, which is consistent with the LIRG-class. Using the Kennicutt (1998) SFR conversion, $\text{SFR} (M_{\odot} \text{ yr}^{-1}) = 4.5 \times 10^{-44} (L_{\text{IR}}/\text{erg s}^{-1})$ (which assumes a starburst age $< 100 \text{ Myr}$ and a Salpeter 1955 initial mass function), yields an average SFR of $(30 \pm 5) M_{\odot} \text{ yr}^{-1}$.

At $z = 0.9$, the MIPS 24 μm band is dominated by a complex of broad polycyclic aromatic hydrocarbon (PAH) emission. When assessing the total L_{IR} , as defined by the 8–1000 μm integrated emission, normalizing template SEDs to 24 μm emission alone is subject to a high degree of uncertainty, due to the potential variation (intrinsic and redshifted)

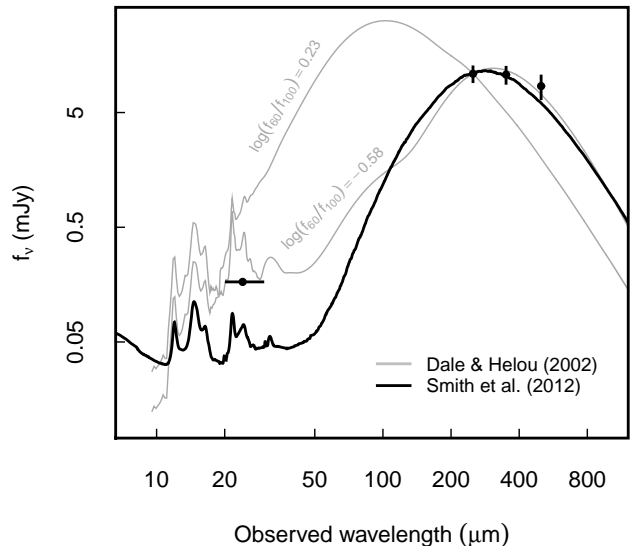


FIG. 3.— SEDs redshifted to $z = 0.9$ and normalized to the average (stacked) 250 μm SPIRE flux at the 14 24 μm cluster members in the filament. Three SED templates have been plotted for illustrative purposes, including the two extremes of the Dale & Helou (2002) library (in terms of the S_{60}/S_{100} color), as well as the Smith et al. (2012) H-ATLAS galaxy template with $1 \times 10^{11} L_{\odot} < L_{\text{dust}} < 3 \times 10^{11} L_{\odot}$. The ‘cool’ color SED templates from Dale & Helou (2002), as well as the H-ATLAS SED are well matched to the average far-IR emission of MIPS-selected emitters in the filament. At $z = 0.9$, the 24 μm band is tracing the rest-frame 13 μm light, which is dominated by a complex of broad PAH emission, thus we expect some variation in SED template matches in this band, as is seen here.

of the PAH contribution in the 24 μm band. Similarly, our lack of spectral coverage in the 30–100 μm range means we have poor constraints on the contribution of a hot dust continuum component, which could boost the luminosity in the 24 μm band (e.g., Fig. 3). This is evidenced by the range of 24 μm fluxes predicted by the 250 μm normalized templates, which straddle the average 24 μm emission. Therefore, we take the Smith et al. (2012) template as a conservative estimate of the form of the RCS 2319+00 members’ SEDs, and use this to calculate the total L_{IR} of the filament.

Since our spectroscopic follow-up of the MIPS cluster members is incomplete, we can only place a conservative lower limit to the total far-IR emission in the filament by summing the 250 μm emission contributed by the 14 24 μm -detected cluster members, yielding $S_{250} = 154 \pm 22 \text{ mJy}$. Assuming each galaxy has the same SED shape, we use the H-ATLAS template to determine a total $L_{\text{IR}} = (2.6 \pm 0.4) \times 10^{12} L_{\odot}$, corresponding to a total SFR within the filament of $(460 \pm 70) M_{\odot} \text{ yr}^{-1}$. We stress that these estimates are strictly lower limits due to the spectroscopic incompleteness of the galaxies in the vicinity of the filament and the requirement of a 24 μm detection. For example, if we include the 27 cluster members that were not detected at 24 μm in the stack, we find a factor of 40% more far-IR emission.

Rather than attempt to correct for spectroscopic completeness we now use a different approach to estimate the total IR emission. Earlier we estimated the statistical total IR excess emission within the filament compared to the average over the map using only the SPIRE data. This should provide a more complete picture of the level of star-formation activity in the

filament as this estimate does not suffer from spectroscopic incompleteness. The total (background subtracted) signal is $S_{250} = 281 \pm 33$ mJy within an area of 26.3 arcmin², which corresponds to a total $L_{\text{IR}} = (4.8 \pm 0.6) \times 10^{12} L_{\odot}$ and SFR within the filament of $\sim 850 \pm 100 M_{\odot} \text{ yr}^{-1}$.

5. DISCUSSION

How can we interpret these observations? First we note that star formation in the filament galaxies is unlikely to be impeded by ram-pressure stripping, given (a) the relatively low density of the intergalactic medium (IGM; Davé et al. 2001) and relative galaxy velocities compared to the cores of the clusters (ram-pressure scales with the ICM density and the square of the galaxy velocity; Gunn & Gott 1972); and (b) the relatively short duration for the star formation events (100s Myr) compared to the time required for stripping in these environments (up to several Gyr, e.g., McCarthy et al. 2008). Furthermore, conditions within intermediate density (i.e., filament) environments might be suitable for tidally inducing activity via close interactions and mergers between gas-rich systems being accreted onto such environments. For example, Geach et al. (2011) find an enhancement in the local fraction of (UV/IR selected) star-forming galaxies in a similar filamentary environment surrounding the Cl0016+16 supercluster at $z = 0.55$. Is the star formation in the RCS 2319+00 supercluster filament significantly enhanced compared to the field?

We have established that the total SFR occurring within the filament, as traced by the $250 \mu\text{m}$ emission, is significantly larger than the local background. On its own, however, this does not directly indicate triggered or enhanced star formation as this may simply reflect the underlying over-density of star-forming galaxies which have not been actively quenched. To quantify any possible enhancement we look at the SFR per unit stellar mass, M_{\star} , or specific SFRs (SSFRs) of the MIPS cluster members in the filament. The stellar mass was derived directly from the measured IRAC- $4.5 \mu\text{m}$ flux densities after applying an ($R_c - z'$) color correction to the M/L ratio, following Bell et al. (2003). Normalized to the same stellar mass, the individual IR galaxies within the filament have $\sim 3 \times$ the SSFR of IR-bright galaxies within the central cluster cores, but only $\sim 1.5 \times$ that of galaxies in the rest of the supercluster. To avoid systematic differences we do not attempt to compare

this to field galaxies at this epoch and simply note that the filament galaxies do not show enhanced emission compared to the rest of the supercluster.

How important would this star formation be to the overall growth of what will be a very massive cluster? Given the apparent low stellar mass of the individual galaxies within the filament, their eventual fate is to fall onto the faint-end of the red sequence. We have estimated the total stellar mass already in place in RCS 2319+00–A within 2.1 Mpc to be $M_{\star} \sim 3 \times 10^{12} M_{\odot}$. This estimate is obtained by fitting a Schechter function to the background-subtracted $4.5 \mu\text{m}$ flux and integrating this to provide a total rest-frame K -band luminosity (above $M_{\text{AB}} \sim -22$) which is then converted to stellar mass assuming an early-type SED (Leitherer et al. 1999). Using the M_{tot} derived from the X-ray luminosity provides a stellar-to-total mass conversion which we then apply to the other two cluster cores, yielding a total $M_{\star} (< 2.1 \text{ Mpc}) \sim 7 \times 10^{12} M_{\odot}$. Thus, if the filament galaxies continue at their current SFRs until the clusters finally merge at $z \sim 0.5$, they will increase the descendent cluster mass by 20%. This should be regarded as an upper-limit, as the star formation will begin to shut down at earlier times as the galaxies enter the increasingly dense cluster environment and as fuel is exhausted; nevertheless the pre-processing witnessed in this filament appears to be an important stage of the build-up of the cluster stellar mass.

ACKNOWLEDGEMENTS

We thank an anonymous referee for a helpful report which improved the paper. We are grateful to Dan Smith for allowing the pre-publication use of the H-ATLAS SED. KEKC acknowledges support from the endowment of the Lorne Trotter Chair in Astrophysics and Cosmology at McGill, the Natural Science and Engineering Research Council of Canada (NSERC), and a L'Oréal Canada Women in Science Research Excellence Fellowship. JEG is supported by a Banting Postdoctoral Fellowship and AF is funded through an NSERC PGSD, both administered by NSERC. TMAW acknowledges support from NSERC. The *Herschel* spacecraft was designed, built, tested, and launched under a contract to ESA managed by the *Herschel/Planck* Project team by an industrial consortium. This work is based in part on observations made with the *Spitzer Space Telescope*, which is operated by JPL, Caltech under a contract with NASA.

REFERENCES

- Bai, L., Rieke, G.H., Rieke, M.J., et al., 2009, *ApJ*, 693, 1840
 Bell, E.F., McIntosh, D.H., Katz, N., Weinberg, M.D., 2003, *ApJS*, 149, 289
 Butcher, H., & Oemler, A., Jr., 1978, *ApJ*, 226, 559
 Butcher, H., & Oemler, A., Jr., 1984, *ApJ*, 285, 426
 Dale, D.A., & Helou, G., 2002, *ApJ*, 576, 159
 Davé, R., Cen, R., Ostriker, J.P., et al., 2001, *ApJ*, 552, 473
 De Lucia, G., Poggianti, B.M., Aragón-Salamanca, A., et al., 2004, *ApJ*, 610, L77
 Eales, S., Dunne, L., Clements, D., et al., 2010, *PASP*, 122, 499
 Egami, E., Rex, M., Rawle, T.D., et al., 2010, *A&A*, 518, L12
 Fazio, G.G., Ashby, M.L.N., Barmby, P., et al., 2004, *ApJS*, 154, 10
 Geach, J.E., Smail, I., Ellis, R.S., et al., 2006, *ApJ*, 649, 661
 Geach, J.E., Ellis, R.S., Smail, I., Rawle, T.D., Moran S.M., 2011, *MNRAS*, 413, 177
 Gilbank, D.G., & Balogh, M.L., 2008, *MNRAS*, 385, L116
 Gilbank, D.G., Yee, H.K.C., Ellingson, E., et al., 2008a, *ApJ*, 673, 742
 Gilbank, D.G., Yee, H.K.C., Ellingson, E., et al., 2008b, *ApJ*, 677, L89
 Gladders, M.D., & Yee, H.K.C., 2005, *ApJS*, 157, 1
 Griffin, M.J., Abergel, A., Abreu, A., et al. 2010, *A&A*, 518, L3
 Gunn, J.E., & Gott, J.R., III, 1972, *ApJ*, 176, 1
 Hicks, A.K., Ellingson, E., Bautz, M., et al., 2008, *ApJ*, 680, 1022
 Hopkins, A.M., & Beacom, J.F., 2006, *ApJ*, 651, 142
 Kennicutt, R.C., 1998, *ARA&A*, 36, 189
 Leitherer, C., Schaerer, D., Goldader, J.D., et al., 1999, *ApJS*, 123, 3
 Marsden, G., Ade, P.A.R., Bock, J.J., et al., 2009, *ApJ*, 707, 1729
 McCarthy, I.G., Frenk, C.S., Font A.S., et al., 2008, 383, 593
 Nguyen, H.T., Schulz, B., Levenson, L., et al., 2010, *A&A*, 518, L5
 Ott, S., 2010, *ASP Conference Series*, 434, 139
 Papovich, C., Momcheva, I., Willmer, C.N.A., et al., 2010, *ApJ*, 716, 1503
 Pascale, E., Ade, P.A.R., Bock, J.J., et al., 2009, *ApJ*, 707, 1740
 Pilbratt, G.L., Riedinger, J.R., Passvogel, T., et al., 2010, *A&A*, 518, L1
 Poggianti, B.M., Desai, V., Finn, R., et al., 2008, *ApJ*, 684, 888
 Rieke, G., Young, E.T., Engelbracht, C.W., et al., 2004, *ApJS*, 154, 25
 Salpeter, E.E., 1955, *ApJ*, 121, 161
 Savage, R.S., & Oliver, S., 2007, *ApJ*, 661, 1339
 Schuster, M.T., Marengo, M., Patten, B.M., 2006, *SPIE*, 6270, 65
 Smith, D.J.B., Dunne, L., da Cunha, E., et al., 2012, *MNRAS*, submitted
 Spergel, D.N., Verde, L., Peiris, H.V., et al., 2003, *ApJS*, 148, 175
 Yee, H.K.C., 1991, *PASP*, 103, 396